*App. Optics*, vol. 8, pp. 1667–1671, Aug. 1969.
[14] S. Iwasa, I. Balslev, and E. Burstein, "The fundamental infra-red lattice vibration spectra of GaAs," *Proc. 7th Int. Conf. Phys. of Semiconductors* (Paris), pp. 1077–1083. (Academic Press, Dunod, 1969.)
[15] A. E. Popa, "Materials study for millimeter subcarrier optical modulators," *IEEE Microwave Theory Tech.* (Int. Symp. 1973), pp. 295–296, 1973.
[16] D. De Nobel, "Phase equilibria and semiconducting properties of cadmium telluride," *Philips Res. Reps.*, vol. 14, pp. 361–399, Jan. 1959.
[17] D. Berlincourt, H. Jaffe, and L. R. Shiozawa, "Electroelastic properties of the sulfides, selenides, and tellurides of zinc and cadmium," *Phy. Rev.*, vol. 129, pp. 1009–1017, Feb. 1963.
[18] S. Yamada, "On the electrical and optical properties of p-type cadmium telluride crystals," *J. Phys. Soc. Japan*, vol. 15, pp. 1940–1944, Nov. 1960.
[19] O. G. Lorimor and W. G. Spitzer, "Infrared refractive index and absorption of InAs and CdTe," *J. App. Phys.*, vol. 36, pp. 1841–1844, June 1965.
[20] B. W. Hakki and P. D. Coleman, "A dielectric resonator method of measuring inductive capacities in the millimeter range," *IRE Trans. Microwave Theory Tech.*, vol. MTT-8, pp. 402–410, July 1960.
[21] W. E. Courtney, "Analysis and evaluation of a method of measuring the complex permittivity and permeability of microwave insulators," *IEEE Trans. Microwave Theory Tech.*, vol. MTT-18, pp. 476–485, Aug. 1970.
[22] Crystal No. 2453, Crystal Specialties, Inc., Monravia, CA.
[23] Crystal No. 4560, Laser Diode Laboratories, Inc., Metuchen, NJ.
[24] Crystal No. 593, II–VI, Inc., Glenshaw, PA.

# Precise Calibration of Plane-Wave Microwave Power Density Using Power Equation Techniques

HOWARD I. BASSEN AND WILLIAM A. HERMAN

*Abstract*—**A power-density calibration methodology utilizing an anechoic chamber, high-power transmitter, and truncated pyramidal horn antenna is described. Plane-wave power density is accurately computed in the far field of the antenna, based upon precise measurements of antenna gain, absolute transmitted power, and multipath reflections. The application of power equation techniques enables direct precise measurements of system mismatches and the accurate transfer of calibration of special bolometers. Several considerations, unique to hazard probe calibrations, are discussed. Absolute power density uncertainties are estimated at 0.56 dB, at 2450 MHz, and 0.76 dB, at 915 MHz, under worst case conditions. A discussion of second-order error sources and their elimination includes the effects of antenna alignment, antenna sidelobes, multipath reflections, field curvature at noninfinite distances, and scattering from test apparatus.**

## I. Introduction

A PLANE-WAVE power-density calibration methodology has been developed. It permits the accurate far-field calibration of hazard probes which are used to measure leakage from microwave ovens, diathermy machines, and other electronic products emitting radiation in the ISM (industrial, scientific, and medical) frequency bands centered at 915 MHz and 2450 MHz. In addition, these probes are extensively utilized to evaluate the levels present in near- and far-field exposure systems used by biological effects researchers. While a few papers have dealt with the problem of hazard probe calibration [1], [2], there is no rigorous treatment of the overall calibration procedure. In particular, little is written dealing with the accurate transfer of primary electrical power standards to the absolute calibration of radiated power-density levels. Therefore, an overall power-density calibration methodology, which deals with direct traceability to a primary electrical standard has been developed, with particular emphasis on the minimization of cumulative errors or uncertainties.

A large body of literature exists, which deals, both analytically and experimentally, with the determination of the gain of standard horn antennas. Additional problems arise when an electrically small antenna such as a hazard probe is introduced into the overall measurement procedure. These problems are not dealt with in most of the previously available literature, and are, therefore, emphasized in this paper. Only plane-wave far-field power-density calibration procedures are developed in this paper. This is a primary factor in the accuracy of all power-density measurement devices. The many near-field measurement problems, unique to specific leakage probes and their inherent antenna/sensor design are not dealt with in this paper, but are discussed elsewhere [3]. This paper describes a technique for the generation of an accurately defined, traceable, and absolute plane-wave power-density level. This enables far-field calibrations to be performed on a wide variety of instruments with a minimum of uncertainty. Extensive use is made of the power equation techniques, developed by Dr. G. Engen of the National Bureau of Standards [4], allowing the

Manuscript received May 25, 1976; revised January 18, 1977.
The authors are with the Electromagnetics Branch, Division of Electronic Products, Bureau of Radiological Health, U.S. Food and Drug Administration, Rockville, MD 20857.

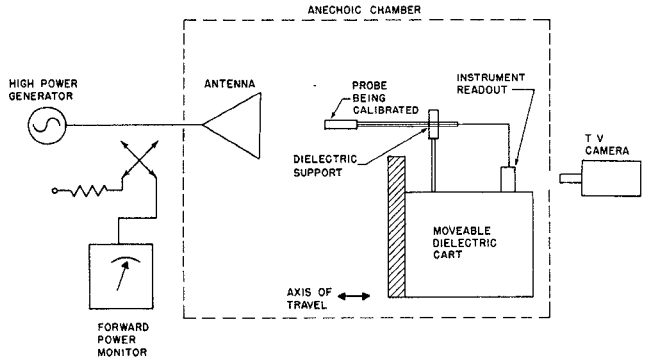


Fig. 1. Probe calibration system.

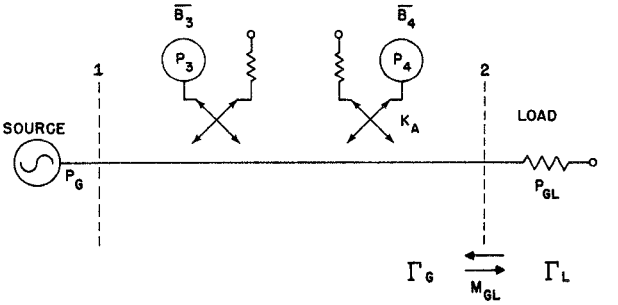


Fig. 2. One-port power equation measurement system.

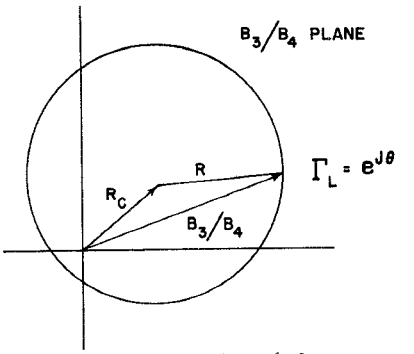


Fig. 3. Power equation relationships.

basic quantities of power and mismatch in a waveguide to be transferred to the calibration of radiated power. Accurate measurement of the path loss between two truncated waveguide horn antennas is performed in an anechoic chamber, facilitating antenna gain determination. A high-power directional coupler, in series with the transmitting antenna, is calibrated to allow absolute transmitted power to be monitored. A small isotropic probe may be placed at a point in the chamber and calibrated, using a television camera with a telephoto lens to observe the instrument's indicated power density (Fig. 1). Evaluation of multipath reflections and other error sources allows the precise prediction of plane-wave power density at this specific point in the chamber.

## II. Power Equation Concepts

The use of power equation concepts permit fast accurate measurements of the total systems mismatch, insertion loss, and absolute power without the restrictive requirements of precision connectors. During these measurements the entire system is treated as a unit, eliminating the characterization of each component with respect to an arbitrary "standard impedance." Cumulative errors associated with the multiple measurements of VSWR, complex impedance, or $S$ parameters are reduced significantly in the specific application to be discussed. The power equation theory and various application techniques have been well documented [4]–[6]. In considering the evaluation of mismatch, it is useful to examine the question of power transfer from a generator/directional-coupler combination to a one-port device (Fig. 2). In this case, using power equation terminology, we have the relationship [4]

$$P_{gl} = P_g M_{gl}. \tag{1}$$

For the above equation, $P_{gl}$ is the net power delivered by the generator to the load, $P_g$ is the available power (the maximum power that can be delivered to a passive load by the generator), and $M_{gl}$ is a matching factor, which may have any value between zero and unity. $P_g$, $P_{gl}$, and $M_{gl}$ are all positive and real. Further, $M_{gl}$ is only a function of the coupler/load combination and is independent of the actual signal source [5]. In more conventional terminology [4]

$$M_{gl} = 1 - \left| \frac{\Gamma_l - \Gamma_g^*}{1 - \Gamma_l \Gamma_g} \right|^2. \tag{2}$$

The parameters above are as follows: $\Gamma_l$ is the reflection coefficient of the load, and $\Gamma_g$ is the reflection coefficient of the equivalent generator associated with the directional coupler. It should be emphasized that $\Gamma_g$ is dependent upon the directivity of the coupler, among other factors.

Furthermore

$$P_g = P_4 k_a. \tag{3}$$

Power $P_4$ represents the coupler sidearm power and $k_a$ is a property of the coupler/sidearm-detector combination. $P_g$, $P_4$, and $k_a$ are all positive and real. It should be noted that $k_a$ is independent of the load at port 2, irrespective of the coupler directivity. In general, $P_g$ is not equal to the power associated with the forward-propagating (generator-to-load) component of the signal in the coupler main arm.

Engen [4] has shown that, if the generator/coupler combination is terminated in a sliding short such that, $\Gamma_l = e^{j\theta}$, the complex voltage ratio, $b_3/b_4$, is described by a circle having a center at $R_c$ and a radius $R$ (Fig. 3), where $b_n \propto P_n^{1/2}$. Thus

$$\left| \frac{b_3}{b_4} \max \right| = \left( \frac{P_3}{P_4} \max \right)^{1/2} = R + |R_c|$$

and

$$\left| \frac{b_3}{b_4} \min \right| = \left( \frac{P_3}{P_4} \min \right)^{1/2} = R - |R_c|. \tag{4}$$

Therefore, by attaching a sliding short to port 2 (Fig. 2) and measuring $b_3/b_4$, the above equations may be solved to obtain values of $R$ and $R_c$ for the particular configuration

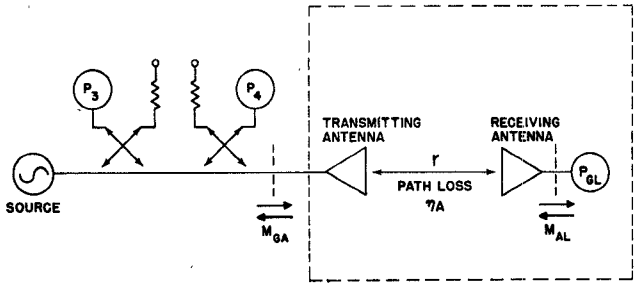


Fig. 4. Path loss measurement system.

measured. Furthermore, it has been shown that, for any passive load

$$M_{gl} = 1 - \left(\frac{|w - R_c|^2}{R^2}\right) \tag{5}$$

where

$$w = b_3/b_4, \qquad \text{for the load of interest.}$$

The parameter $M_{gl}$, in (1), can be unambiguously determined by values of $w$, $R_c$ (complex quantities), and $R$. If phase measurement capabilities are not available, a tuner must be used to eliminate either $w$ or $R_c$. In the present application, offset waveguide shorts, together with phase and amplitude data, provide the capability for rapid multifrequency measurements in each ISM band. Computation of $M_{gl}$ is performed from this data. When measuring the path loss between antennas (Fig. 4) via power equation techniques, the magnitude of the loss is large enough (> 15 dB) to allow a one-port mismatch measurement to be performed independently, on both transmitting and receiving antennas. Path loss ($\eta_a$) may be computed from the relationship

$$\eta_a = \frac{P_{gl}}{P_4 k_a M_{ga} M_{al}} \tag{6}$$

where $M_{ga}$ and $M_{al}$ are matching factors of the transmitting and receiving antennas, respectively. The effects of chamber surface and antenna support structure reflections are included in the measurement of matching parameters. Other parameters are illustrated in Fig. 4 for the path loss measurement.

## III. Antenna Gain Measurement

The relationship employed in the calibration of far-field power density ($S$) is

$$S = \frac{P_T G_T}{4\pi r^2} \tag{7}$$

where the transmitted power ($P_T$) and distance ($r$) from an antenna with far-field gain, $G_T$, are measured quantities [7]. For noninfinite separations between the pair of antennas, a "near-zone correction factor" must be applied to the far-field gain of the antennas [8]. This factor has a value of less than one, and increases with separation distance, approaching unity as a limit. As long as antenna separations are greater than many units of $a^2/\lambda$ (where $a$ is the maximum aperture dimension of the larger antenna and $\lambda$ is the wavelength of the transmitted signal), plane-wave power density may be computed, using (7) where $G_T$ is the product of the constant far-field gain and the near-zone correction factor ($G_T$ is a function of distance). This separation criterion ensures that no transmitting antenna reactive fields are intercepted by the receiving antenna, and only second-order field curvature effects are corrected for.

Using a total of three antennas, in three combinations of two antennas per path loss measurement, individual antenna gains may be computed from the relationship

$$G_T G_R = \frac{P_R}{P_T}\left(\frac{4\pi r}{\lambda}\right)^2 \tag{8}$$

where $(P_R/P_T) = \eta_a$, as previously defined. The reciprocity of antennas is assumed, implying that gain is not dependent upon the role of the antenna (transmitting or receiving) or its physical environment (assuming sidelobe reflections are negligible). Experimental tests were performed to ensure that the separation distances between antennas were sufficient to justify the "plane wave" and the reciprocity assumptions.

## IV. Absolute Transmitted Power Calibration

It is required that plane-wave power densities be generated with magnitudes sufficient for the calibration of typical microwave hazard survey instruments (1–10 mW/cm$^2$) at distances from the transmitting antenna which satisfy previous theoretical assumptions. Therefore, high powers (up to 1 kW) must be transmitted. A convenient, and highly accurate, secondary standard of absolute microwave power is the coaxial bolometer, calibrated as a function of dc substituted power for a given net microwave input power (1 mW) with a self-balancing bridge. To establish a high power-density level in the far field of a horn antenna, much larger amounts of power must be accurately measured with respect to this reference. A cascaded directional coupler technique [9] may be used to obtain accurate 100–1000-W calibrated power measurements. A unitized, "high-power meter," separate from the power-density calibration system, was created for use as a high-power reference standard. This "high-power meter" serves as a transfer standard, tying the power-density calibration system to the precisely calibrated 1-mW-reference bolometer, previously mentioned. When used in conjunction with power equation techniques, a minimum amount of cumulative errors exist in the transfer of calibration procedures from the electric standards laboratory to the power-density calibration facility. These coupler/bolometers have been precisely calibrated by the National Bureau of Standards for effective efficiency (the ratio of dc substituted power in the bolometer to net microwave power). The calibration of transmitted power involves the use of the subsystems shown in Fig. 5. The subsystems are: a transmitting antenna, the calibrated coupler/bolometer, a forward power monitor (consisting of a rigid high-power transmission line with an integral directional coupler, sidearm power meter, and waveguide output port), a set of three waveguide offset short circuits, and an

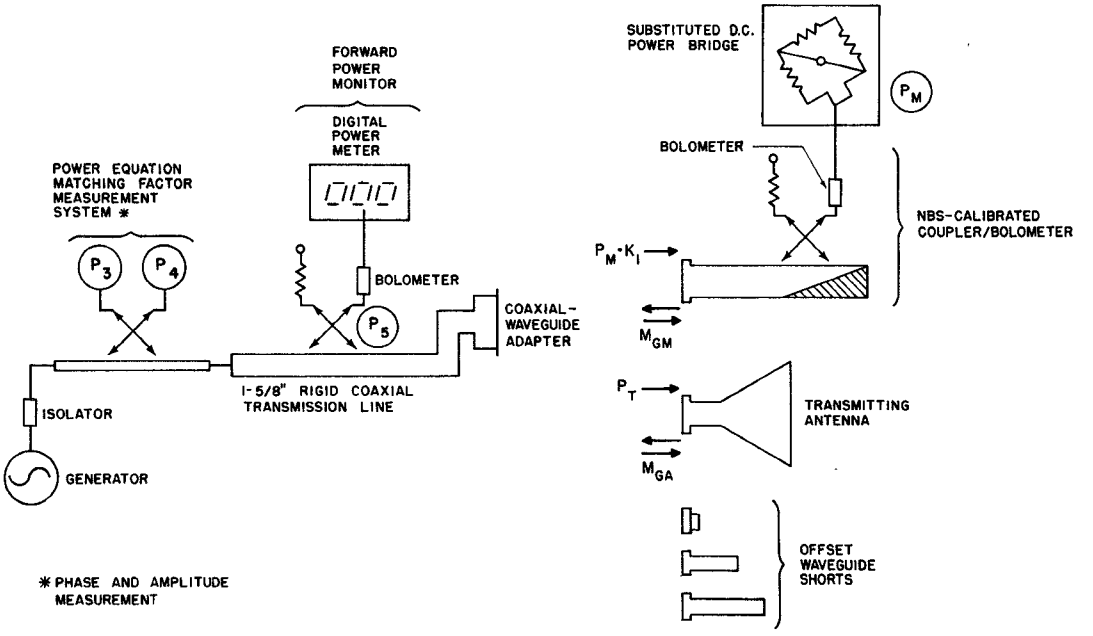


Fig. 5. Absolute transmitted power calibration.

additional pair of directional couplers to measure matching factors. Only the antenna and forward power monitor are used in the final system operation (Fig. 1).

During the calibration procedure, the forward power monitor is first terminated by the calibrated coupler/bolometer. The reading of the power meter ($P_4$) on the first set of directional couplers and the value of substituted dc power applied to the previously calibrated reference coupler/bolometer are simultaneously recorded. The coupler/bolometer's matching factor ($M_{gm}$) is measured next, via power equation techniques involving the use of the offset shorts. The next step is to terminate the system with the transmitting antenna, and to measure $M_{ga}$, the match to the antenna. Finally, simultaneous values of $P_4$ and $P_5$ (where $P_5$ is the meter reading of the forward power monitor), are also recorded with the antenna in place. The linearity of $P_4$ and $P_5$ must be accounted for, when various power levels are to be transmitted. The net power, fed to the transmitting antenna ($P_T$), is expressed as

$$P_T = \frac{P_m k M_{ga}}{M_{gm}} \tag{9}$$

where $P_m$ is the substituted dc power applied to the bolometer to restore its original resistance (as measured before microwave generation). In addition, $k$ is defined as the effective efficiency of the coupler/bolometer. Parameters $M_{gm}$ and $M_{ga}$ are matching factors which were previously defined. During this procedure, the power, $P_4$, is held constant while the coupler/bolometer, and then the antenna, terminate the system (implying that $P_G$ is constant, from (3)).

## V. Laboratory Measurement Techniques

Power-equation matching-factor measurements were performed on transmitting and receiving antennas using the one-port power equation model for each antenna. The lack of significant mutual interaction between antennas was experimentally verified by placing a sliding short circuit on the output of the transmitting antenna (outside of the anechoic chamber). The minimum possible antenna separation was established and the receiving antenna matching factor, $M_{al}$, was measured. Continuous movement of the sliding short over several wavelengths produced variations of less than 1 percent in $M_{al}$. This test was more severe than the actual situation where both antennas are terminated in well-matched loads.

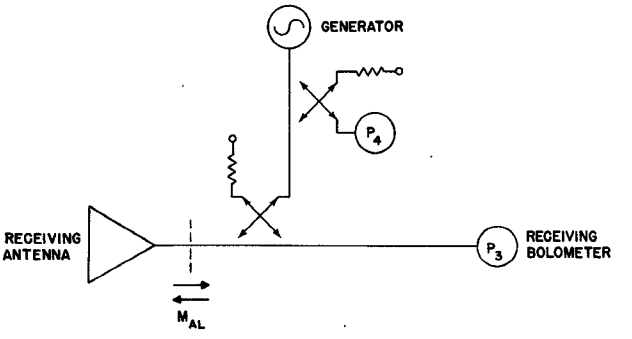


Fig. 6. Receiving antenna measurement system.

The receiving antenna measurement configuration is shown in Fig. 6 as described by Engen [5]. It was mounted on foam blocks several wavelengths above a dielectric cart, in the anechoic chamber. Reflections from the transmitting wall of the chamber, as seen by the receiving antenna were significant, because of the close proximity of this wall to the transmitting antenna. The receiving antenna matching factor, $M_{al}$, was measured as a continuous function of antenna separation distance. In contrast, the transmitting antenna matching factor was found to be insensitive to cart position because of the minimal scattering cross section of the cart and receiving horn.

Path loss measurements were performed with a precision bolometric ratiometer. First, the zero-path loss case was established by removing both antennas from their respective mounts. The transmitting and receiving waveguides were bolted together, and both the mismatch and the received to transmitted power ratio were measured. Path loss between antenna pairs was plotted as a function of distance using an accurate cart position encoder. Chamber multipath reflections were minimal (less than 0.1 dB) because of the careful selection of the proper directivity of antennas and good chamber design. Antenna sidelobe radiation effects and leakage from transmission line connectors were checked for and eliminated by various experimental techniques. Both antennas were carefully aligned so that their mechanical boresight axis coincided with the chamber's central axis. Alignments were performed with a laser, rigidly mounted outside the chamber. Its beam was transmitted through the rear wall, parallel to both the chamber's center axis and the rails on which the dielectric cart rides. Special waveguide inserts containing a first-surface mirror were placed in each antenna to enable their alignment with the chamber's center axis.

## VI. Hazard Probe Calibration

Multipath effects due to chamber wall reflections can cause significant calibration errors when low-gain antennas, such as those used in a microwave hazard probe, are exposed at large distances from the transmitting antenna. These reflections may be accounted for, and their effects eliminated as follows. The probe in question is placed on a movable dielectric cart and its received power-density indication is plotted as a continuous function of distance to the transmitter. Periodic oscillations appearing on the plot represent multipath effects. Since cart position can be precisely repeated, any probe with nominally identical antenna characteristics may be calibrated, and multipath errors corrected for, as a function of distance to the transmitting antenna, based on the knowledge of the magnitude of the oscillations. Reflections from the cart and dielectric support structures which hold the probe, produce additional errors that cannot be detected by moving the cart and probe with respect to the transmitting antenna. A technique was devised to minimize these reflections. Cart reflections may be quantified by varying the cart position, while observing the net-field-strength standing waves with a stationary isotropic probe, of the type to be calibrated. The probe in this case is not on the cart, but is mounted in the center of the chamber between the transmitting antenna and the cart, intercepting the chamber's center axis. Absorbing material is added to the cart, until the reflections, as seen by the probe, are minimized. This technique has been utilized not only to quantify cart reflections, but to facilitate the measurement of reflections from various dielectric objects [10].

Although cart reflections may be reduced through the use of absorber material, second-order errors of several percent remain, when a probe is placed on the cart at a great distance from the transmitting antenna. Since the position of standing waves in the observed field strength is known for a

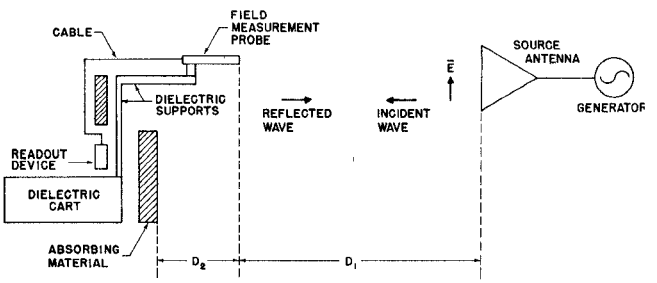


Fig. 7. Multiposition averaging technique.

stationary probe, placed ahead of the cart, "multi-position averaging" over a number of cycles of the standing waves may be used to greatly reduce residual errors, due to cart and probe support reflections. The distance $D_2$ is varied in half-cycle increments of the standing wave (Fig. 7) while distance $D_1$ is reset to the same value for all measurements. The distance corresponding to one cycle of the standing waves was found to be exactly one half of a wavelength, because of the straight-line reflection path from the cart to the probe. Numerical averaging of the indicated power density of the probe was performed for four or more values of $D_2$ (each one-quarter wavelength greater than the previous value). This resulted in enhanced accuracy, and excellent repeatability of calibration (better than 3 percent).

The assumption was previously made that the separation, between the transmitting antenna (truncated pyramidal horn) and receiving antenna (either an identical horn or small probe), was sufficient to ensure negligible amplitude and phase curvature of the received field. If this were not the actual case, spatial averaging, over the large aperture of the receiving horn, would occur during gain measurement. This would introduce an error in the calibration of a small probe when the latter was positioned on the boresight of the transmitting antenna because of the small "effective aperture" of the probe. The worst case occurs in the lower frequency range (915 MHz) where a separation of only 6.5 $a^2/\lambda$ exists in the center of the chamber. To estimate field curvature, experimental scanning over a plane normal to the axis of propagation was performed with an electrically small probe. Numerical integration of data yielded a "spatially averaged" power-density value over an area defined by the physical dimensions of the receiving horn. (The receiving antenna was removed from the chamber during the scanning process.) A comparison of this "spatially averaged" value with the single "spatial peak" value obtained at the geometric center of the plane was made. The ratio of "spatial peak" to "average" power density was 0.95 at the above separation. Since the horn antenna's "effective aperture" is considerably smaller than its physical aperture, an error of less than 0.05 dB is estimated due to noninfinite antenna separation after an approximate correction factor is assigned to subsequent calibrations.

## VII. Error Analysis

The uncertainties involved in the power-density calibration system may be divided into three main categories: 1) uncertainties associated with the horn gain measurements,

TABLE I
PLANE-WAVE POWER-DENSITY CALIBRATION SYSTEM UNCERTAINTIES

| Measurement | Worst Case Uncertainty (Optimum System) 915 MHz | 2450 MHz |
|---|---|---|
| Antenna Path Loss | (dB) | (dB) |
| Distance Measurement* | .01 | .01 |
| Ratiometer Nonlinearity | .05 | .05 |
| Mismatch Measurements | .05 | .05 |
| Multipath Effects and Scattering | .15 | .05 |
| Antenna Alignment | .02 | .05 |
| Error Summation - Antenna Pair | .28 | .21 |
| Net Gain Uncertainty - Single Antenna | .42 = $\varepsilon_A$ | .32 = $\varepsilon_A$ |
| Absolute Transmitted Power | | |
| Coupler/Bolometer Calibration* | .09 | .09 |
| Transfer Error | .05 | .05 |
| Mismatch Measurements | .05 | .05 |
| Total Transmitted Power Uncertainty | .19 = $\varepsilon_P$ | .19 = $\varepsilon_P$ |
| Isotropic Probe Calibration | | |
| Residual Chamber Multipath | .05 | .02 |
| Residual Cart Reflections | .05 | .02 |
| Field Curvature (non-infinite separation) | .05 | .01 |
| Total Probe Calibration Uncertainty | .15 = $\varepsilon_I$ | .05 = $\varepsilon_I$ |
| Total Calibration System Uncertainty ($\varepsilon_A+\varepsilon_P+\varepsilon_I$) | .76 | .56 |

*Using NBS-calibrated transfer standards.

2) uncertainties associated with the calibration of the forward power monitor, and 3) multipath effects for an isotropic probe calibration. The gain measurements involve uncertainties in antenna mismatches, separation distances, and path loss measurements (including multipath effects).

The error analysis (Table I) presents the worst-case uncertainty levels that occur in an optimum system. The values are conservative, and because of the random nature of many measurement errors, an actual absolute power-density calibration, performed with the optimum system, is probably more accurate than presented.

## APPENDIX
## SINGLE ANTENNA GAIN MEASUREMENT UNCERTAINTY COMPUTATION FOR THE THREE ANTENNA METHOD

The gain of a single antenna ($G_1$) is computed from the gain product derived in (8) as

$$G_1 = \sqrt{\frac{(G_1G_2)(G_1G_3)}{G_2G_3}} \tag{10}$$

where

$G_n$ gain of antenna $n$ (a computed value);
$G_nG_m$ gain product of a pair of antennas (a function of the measured path loss).

If the worst case uncertainty ($\varepsilon_n$) is included in the measured values, the following expression results:

$$G_1 = \sqrt{\frac{G_1G_2(1\pm\varepsilon_1)G_1G_3(1\pm\varepsilon_2)}{G_2G_3(1\pm\varepsilon_3)}} \tag{11}$$

$\varepsilon_1 \simeq \varepsilon_2 \simeq \varepsilon_3 = \varepsilon$, since these uncertainties involve the identical measurement system and $G_1G_2$ is very close in value to $G_1G_3$ or $G_2G_3$ for nominally identical antennas.

Then the gain for a single antenna is

$$G_1 = \sqrt{\frac{(G_1G_2)(G_2G_3)}{G_2G_3}}\sqrt{\frac{(1+\varepsilon)(1+\varepsilon)}{(1-\varepsilon)}} \tag{12}$$

since $\varepsilon^2 \ll 1$

$$G_1 \simeq (1+\varepsilon)^{3/2}\sqrt{\frac{(G_1G_2)(G_1G_3)}{G_2G_3}}. \tag{13}$$

Thus the worst case uncertainty for $G_1$ is

$$\varepsilon_G = (1+\varepsilon)^{3/2} - 1. \tag{14}$$

## ACKNOWLEDGMENT

The assistance of Dr. G. Engen, E. Komarek, and P. Hudson of the National Bureau of Standards enabled the precise calibration of power and mismatch in the various systems employed. The following Bureau of Radiological Health staff members assisted in the program: the preliminary measurements and analysis performed by M. Swicord and the theoretical investigations performed by S. Neuder are acknowledged. The mechanical and electronic development of the chamber rail system and laser alignment system were performed by J. Duff and J. Bing.

## REFERENCES

[1] D. Woods, "Standard intensity electromagnetic field installation for calibration of radiation hazard monitors from 400 MHz to 40 GHz," *Non-Ionizing Radiation*, pp. 9–17, June 1969.
[2] R. C. Baird, "Methods of calibrating microwave hazard meters," in *Biological Effects and Health Hazards of Microwave Radiation Symposium Proceedings*. Warsaw, Poland: Polish Medical Publishers, 1974, pp. 228–236.
[3] M. Swicord, H. Bassen, W. Herman, J. Duff, and J. Bing, "Methods and instrumentation for the evaluation and calibration of microwave survey instruments," in *Selected Papers of the USNC/URSI Annual Meetings*, vol. II, DHEW Publication FDA 77-8011, Dec. 1976 (Boulder, Colorado, Oct. 20–23, 1975).
[4] G. F. Engen, "An introduction to the description and evaluation of microwave systems using terminal invariant parameters," National Bureau of Standards, Monograph 112, Oct. 1969.
[5] ——, "Theory of UHF and microwave measurements using the power equation concept," *National Bureau of Standards Technical Note 637*, Apr. 1973.
[6] ——, "Power equations: a new concept in the description and evaluation of microwave systems," *IEEE Transactions on Instrumentation and Measurements*, vol. IM-20, no. 1, pp. 50–57, Feb. 1971.
[7] J. D. Kraus, *Antennas*. New York: McGraw-Hill, 1950, pp. 41–56.
[8] R. Bowman, "Field strength above 1 GHz: measurement procedures for standard antennas," *Proceedings IEEE*, vol. 55, no. 6, pp. 980–991, June 1967.
[9] K. Bramall, "Accurate microwave high power measurements using a cascaded coupler method," *National Bureau of Standards Journal of Research*, vol. 75c, no. 3-4, Dec. 1971.
[10] J. C. Lin and H. Bassen, "Perturbation effect of animal restraining materials on microwave exposure," *IEEE Transactions on Biomedical Engineering*, vol. BME-24, pp. 80–83, Jan. 1977.